Molecules **2009**, *14*, 3115-3131; doi:10.3390/molecules14093115

OPEN ACCESS

molecules

ISSN 1420-3049

www.mdpi.com/journal/molecules

Review

Solid State Polyselenides and Polytellurides: A Large Variety of Se–Se and Te–Te Interactions

Christian Graf, Abdeljalil Assoud, Oottil Mayasree and Holger Kleinke *

Department of Chemistry, University of Waterloo, Waterloo, ON, N2L 3G1, Canada

* Author to whom correspondence should be addressed; E-mail: kleinke@uwaterloo.ca.

Received: 7 July 2009; in revised form: 15 August 2009 / Accepted: 19 August 2009 / Published: 24 August 2009

Abstract: A large variety of different interactions between the chalcogen atoms, *Q*, occur in the solid state structures of polyselenides and polytellurides, including both molecular and infinite units. The simplest motifs are classical Q_2^{2-} dumbbells and nonlinear Q_n^{2-} chains (n = 3, 4, 5, ..), e.g. found in alkali metal polychalcogenides. In addition, nonclassical so-called hypervalent motifs exist in the form of linear Q_3^{4-} units or within larger units such as Q_4^{4-} and Q_5^{4-}. Infinitely extended *Q* units include zigzag, *cis*/*trans* and linear chains, as well as planar and slightly puckered layers. Several of those are susceptible to Peierls distortions, leading to the formation of both commensurate and incommensurate superstructures and anomalies in transport properties, including metal-nonmetal transitions.

Keywords: selenium; tellurium; bonding; hypervalent

1. Introduction

Solid state materials based on chalcogenides, *i.e.*, sulfides, selenides and tellurides, play a large role in today's society. Examples include semiconductor devices, e.g. in solid state electronics [1], fast-ion conductors [2,3], rechargeable batteries [4], data storage including phase-change materials [5-7], chalcogenide glasses [8], and the thermoelectric energy conversion [9-12]. Polychalcogenides, like the potential thermoelectric material $HfTe_5$, are materials that comprise homonuclear bonds between negatively charged chalcogen atoms, e.g. a Se–Se bond within Se_2^{2-} pairs of Rb_2Se_2 [13]. These bonds occur in chalcogen-rich materials, where the chalcogen atom cannot be reduced to attain the closed-shell formation as in Q^{2-}. For example, Se carries a charge of –1 in Rb_2Se_2, like O in SrO_2, and

therefore forms one Se–Se bond. As such, Rb_2Se_2 is a typical Zintl phase. Zintl phases AX_x consist of an electropositive element *A* (here: Rb) and a more electronegative element *X* of the later (post transition) main groups (here: Se). Assuming a complete charge transfer of all of *A*'s valence-electrons to *X*, the cation A^{z+} possesses a full octet, and the (formal) anion $X^{z/x-}$ attains the octet by forming homonuclear *X*–*X* bonds in addition to the reduction by *A*. In most cases, these bonds are classical single bonds (two-center two-electron, *2c-2e*), i.e. exactly one bond is formed for each electron missing to complete the octet of *X* [14-16].

The rich structural chemistry in particular of the polyselenides and polytellurides is the scope of this review, going beyond the common *2c-2e* bonds: hypervalent interactions as found in XeF_2 [17] or SF_6 [18] are often observed in various fragments of these materials [19]. In addition, weaker fractional bonds or cohesive interactions of different lengths, as in elemental tellurium, render the Se/Te substructures intriguingly complex [20,21], which in turn may be beneficial for the thermoelectric energy conversion [22]. Four reviews about polychalcogenides from the years 1995 to 2000 underline the importance of this field [20,23-25].

2. Results and Discussion

2.1. Molecular units in polyselenides and polytellurides

2.1.1. Oligomeric Q_n^{2-} motifs

The simplest polychalcogenide motif is the dumbbell unit Q_2^{2-}, occurring for example in Na_2Se_2 [26], Rb_2Se_2 and Rb_2Te_2 with Se–Se and Te–Te distances of 2.38 Å, 2.47 Å and 2.78 Å, respectively (Figure 1). These dumbbells are also found in organic compounds with similar bond lengths, e.g. in $[N(CH_3)_4]_2Te_2$ (d_{Te-Te} = 2.74 Å) [27] and $[Na(CH_3OH)_3]_2Te_2$ [28]. Assigning charges is straightforward in these examples, e.g. $(Na^+)_2Se_2^{2-}$, with Se_2^{2-} being isoelectronic to Br_2 and I_2, with 14 valence-electrons for the dumbbells, which are therefore held together by one *2c-2e* bond. While generally these distances compare well with the sum of the single bond radii, r_{Se} = 1.17 Å and r_{Te} = 1.37 Å [29], the influence of the cations is evident, for the Se–Se bond in Rb_2Se_2 is approximately 0.1 Å longer than in Na_2Se_2.

Figure 1. From left to right: Oligomeric Q_n^{2-} motifs in Na_2Se_2, K_2Se_3, Na_2Se_4, and K_2Se_5.

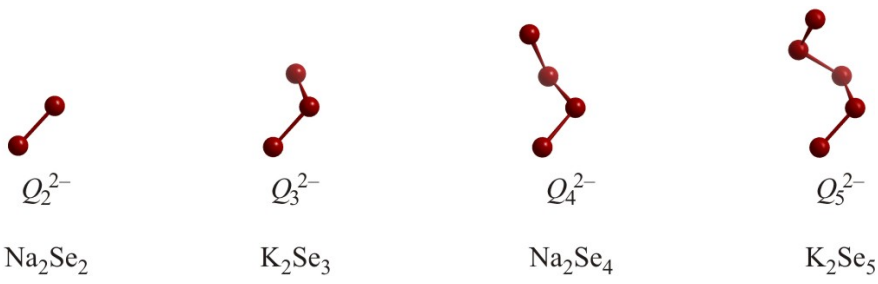

The dumbbells can formally be extended to oligomeric chain-like units Q_n^{2-} (with *n* = 3, 4, 5, 6, 12, 13) by adding neutral *Q* atoms to the chain, wherein the terminal *Q* atoms remain negatively charged. Each neutral *Q* atom participates in two *2c-2e* bonds, comparable to the elemental structures of

selenium and tellurium. Se_3^{2-} groups (with one central neutral Se atom) occur for example in, K_2Se_3 [30], Sr_2SnSe_5 [31] and Ba_2SnSe_5 [32], with bond lengths of approximately 2.4 Å, and Te_3^{2-} groups in K_2Te_3 with d_{Te-Te} = 2.80 Å [33] and in $Ba_7Au_2Te_{14}$ with d_{Te-Te} = 2.89 Å [34]. It is evident that the lengths of regular single (*2c-2e*) bonds may vary substantially, noting that these bonds are significantly elongated compared to 2× r_{Se} = 2.34 Å and 2× r_{Te} = 2.74 Å, respectively.

The Q_3^{2-} anions are bent, ideally exhibiting C_{2v} symmetry, with typical *Q*–*Q*–*Q* bond angles of 105° - 110°, in accordance with the VSEPR concept, which suggests tetrahedral arrangement of the two bonds and two free electron pairs around the central *Q* atom. The packing of the three-dimensional structure may cause a severe distortion of the angle as well, e.g. down to 92° in $Ba_7Au_2Te_{14}$.

Anions with larger *n*, such as Se_4^{2-} in Na_2Se_4 (d_{Se-Se} = 2.35 Å and 2.36 Å) [35], Te_4^{2-} in $(Ph_4P)_2Te_4{\cdot}2CH_3OH$ (d_{Te-Te} = 2.72 Å and 2.76 Å) [36], Se_5^{2-} in K_2Se_5 (2.34 Å ≤ d_{Se-Se} ≤ 2.37 Å) [37], and Se_6^{2-} in $[Me_3N(CH_2)_{13}CH_3]Se_6$ (2.27 Å ≤ d_{Se-Se} ≤ 2.35 Å) [38] are best described as oligomeric zigzag or helical chain fragments. Larger chain-like polychalcogenide anions, though extremely rare, do exist, like Te_{12}^{2-} in $[N(C_2H_5)_4]_2Te_{12}$ [39] and Te_{13}^{2-} in Cs_2Te_{13} [40] (Figure 2), and they are often - as in these two examples - interconnected via longer interchain interactions (here: 3.14 Å and 3.18 Å). These interactions are much shorter than twice the van der Waals radius and will be discussed later in this review.

Figure 2. Oligomeric Te_n^{2-} motifs in $(NEt_4)_2Te_{12}$ (left) and Cs_2Te_{13} (right).

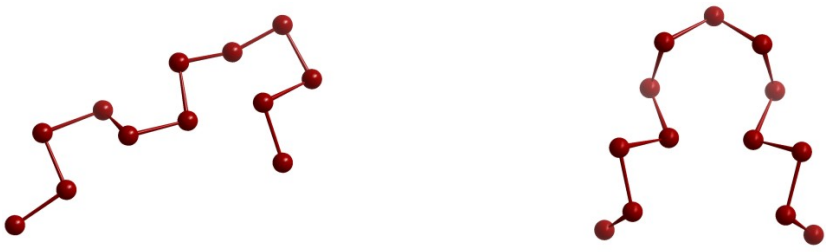

Te_{12}^{2-} Te_{13}^{2-}

$(NEt_4)_2Te_{12}$ Cs_2Te_{13}

2.1.2. Oligomeric Q_n^{4-} motifs

Since the Q_n^{4-} fragments comprise two more valence-electrons than their Q_n^{2-} counterparts, they cannot contain the same *2c-2e* bonds. *n* = 2 is a hypothetical case only, as it would correspond to two isolated closed-shell Q^{2-} anions. *n* = 3 is realized in Se_3^{4-} units of $Ba_2Ag_4Se_5$ [41], and $Rb_{12}Nb_6Se_{35}$ [42]. In the former, Se_3^{4-} exhibits the highest symmetry possible, namely linearity and equidistant interactions, thus point group $D_{\infty h}$, while $Rb_{12}Nb_6Se_{35}$ is comprised of two differently distorted, almost linear Se_3^{4-} units of C_{2v} and C_1 symmetry, respectively. In these two compounds, the Se–Se–Se bond angle of Se_3^{4-} varies between 180° and 164°, and the Se–Se bond lengths between 2.59 Å and 2.77 Å (Figure 3).

Figure 3. From left to right: Se_3^{4-} ($D_{\infty h}$), Se_3^{4-} (C_{2v}), Se_4^{4-}, *cis*-Se_5^{4-} and *trans*-Te_5^{4-}.

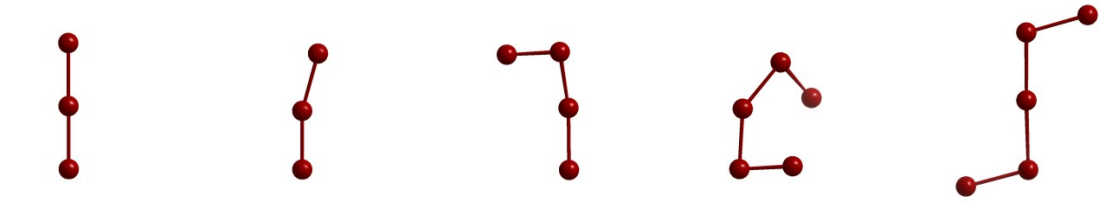

Se_3^{4-} Se_3^{4-} Se_4^{4-} Se_5^{4-} Te_5^{4-}

$Ba_2Ag_4Se_5$ $Rb_{12}Nb_6Se_{35}$ $K_3CuNb_2Se_{12}$ Nb_2Se_9 Ba_2SnTe_5

$Ba_2Ag_4Se_5$ contains two isolated Se^{2-} anions and one Se_3^{4-} per formula unit, according to the ionic formulation $(Ba^{2+})_2(Ag^+)_4Se_3^{4-}(Se^{2-})_2$. Electronic structure calculations and electrical conductivity measurements confirmed the semiconducting, hence electron precise character of this compound [41]. $Rb_{12}Nb_6Se_{35}$ is a special case, containing both Se_3^{2-} and Se_3^{4-} units, according to the formula $(Rb^+)_{12}(Nb^{5+})_6(Se_3^{2-})_2(Se_2^{2-})_7(Se_3^{4-})_3(Se^{2-})_6$. Since diffuse reflectance measurements supported the semiconducting and thus closed-shell character of $Rb_{12}Nb_6Se_{35}$ [42], this treatment of $Rb_{12}Nb_6Se_{35}$ within the Zintl concept is justified.

With 22 valence-electrons, Se_3^{4-} is isoelectronic with hypervalent linear XeF_2 and I_3^-. Several examples are known that contain the linear I_3^- motif, including CsI_3 [43] and $[Ph_4As]I_3$ [44]. Ideally the two I–I distances are equivalent, with a bond angle of 180° as in $[Ph_4As]I_3$ (d_{I-I} = 2.90 Å), but deviations from the centrosymmetric arrangement are often found with smaller cations, like in CsI_3 with I–I bonds of 2.84 Å and 3.04 Å and a bond angle of 178°. The linear arrangement is well understood based on Rundle's model [45], which treats the *s* orbitals as well as the *p* orbitals of π symmetry as lone pairs. Then the frontier orbital set consists of one filled σ bonding, one filled nonbonding, and one empty σ antibonding molecular orbital, formed by the p_z orbitals when *z* corresponds to the molecular axis. The nonbonding orbital contains a nodal plane at the center of the triatomic unit, resulting in a three-center-four-electron (*3c-4e*) bond. The validity of Rundle's model was - in principle - confirmed for Se_3^{4-} via Gaussian calculations using the B3LYP functional [41].

Since the *3c-4e* bonds are electron deficient, containing only one bonding molecular orbital for two bonds (which is why they are often called "half" bonds), they are longer than the regular *2c-2e* bonds. Correspondingly, the I–I single bond in I_2 of 2.76 Å is much shorter than the above-mentioned I–I bonds (2.84 Å and 3.04 Å), and Se–Se single bonds (2.34 Å) are shorter than the Se–Se bonds of Se_3^{4-} (2× 2.77 Å in $Ba_2Ag_4Se_5$ and 2.59 Å - 2.65 Å in $Rb_{12}Nb_6Se_{35}$). In $Rb_{12}Nb_6Se_{35}$, the bond angles of approximately 164° deviate substantially from linearity, which is likely caused by the packing effect. Despite the distortion, the Se_3^{4-} unit of $Rb_{12}Nb_6Se_{35}$ can easily be distinguished from the Se_3^{2-} unit occurring in the same structure, which shows bond distances of 2.39 Å and a bond angle of 94°.

While no isolated, linear hypervalent Te_3^{4-} anion has been reported so far, the isoelectronic linear units P_3^{7-}, As_3^{7-}, Sb_3^{7-}, and Bi_3^{7-} all occur in the numerous representatives of the $Ca_{14}AlSb_{11}$ type [46], including $Ca_{14-x}Eu_xMnSb_{11}$, which exhibits colossal magnetoresistance [47], and the high temperature thermoelectric $Yb_{14}MnSb_{11}$ [48].

The only Q_4^{4-} representative known to date is Se_4^{4-} in $K_3CuNb_2Se_{12}$ [49], which is basically an almost linear Se_3^{4-} unit (bond angle: 166°) with an additional Se atom attached via a single bond to one

end. Therefore, its ideal valence-electron number is 28, namely 22 for the Se_3^{4-} fragment plus six for the additional Se atom. Within this model, we interpret the two bonds of the linear part as *3c-4e* bonds and the exo bond as *2c-2e*. This is in accord with the 2.73 Å and 2.54 Å distances for the (*pseudo*) collinear bonds, and the short 2.39 Å bond to the fourth Se atom with a bond angle of 93°. $K_3CuNb_2Se_{12}$ is another example for a complex selenide with three topologically different Se units, namely tetrameric Se_4^{4-}, Se_2^{2-} pairs, and isolated Se^{2-}, according to $(K^+)_3Cu^+(Nb^{5+})_2Se_4^{4-}(Se_2^{2-})_3(Se^{2-})_2$.

Representatives for Q_n^{4-} with $n = 5$ exist both among selenides and tellurides. In all cases, the Q_5^{4-} units contain a central (almost) linear hypervalent unit, with the two remaining *Q* atoms attached via a single bond to both ends of the linear part, like the fourth atom in Se_4^{4-}. By analogy, we conclude an ideal valence-electron number of 34, namely 22 for the Q_3^{4-} fragment plus 2× six for the two additional *Q* atoms, hence Q_5^{4-}: 5× 6 valence-electrons (from the neutral *Q* atoms) plus four for the negative charges equals 34.

The two terminal *Q* atoms may be in *cis* or *trans* conformation. The *cis* variant is realized in the heavily distorted Se_5^{4-} of Nb_2Se_9, wherein the hypervalent bonds of 2.64 Å and 2.66 Å exhibit a bond angle of only 143°, and the terminal single bonds of 2.36 Å/2.37 Å are both connected with a 83° bond angle. Considering the presence of a 2.90 Å Nb–Nb bond, Nb is most likely in the 4+ state, and noting the presence of two Se_2^{2-} pairs per formula unit, $(Nb^{4+})_2Se_5^{4-}(Se_2^{2-})_2$ is also a closed-shell material [50].

The *trans* conformation is only known within the tellurides, occurring in NaTe ($(Na^+)_6Te_5^{4-}Te^{2-}$) [51] and Ba_2SnTe_5 ($(Ba^{2+})_6(Sn^{4+})_3Te_5^{4-}(Te^{2-})_{10}$) [52]. An isoelectronic cationic variant is I_5^+ in I_5AsF_6 [53], while analogous pnictides have not been reported yet.

The largest representative of the series Q_n^{4-} currently known is Te_7^{4-}, coordinated to an Ag^+ or Hg^{2+} cation via the central Te and the two terminal Te atoms [54,55]. The Te_7^{4-} anion can formally be constructed from adding two neutral Te atoms to a *cis*-Te_5^{4-}. In case of the Ag compound, the central Te_3 unit contains hypervalent bonds of 2.87 Å and 3.23 Å with a bond angle of 174°, and the additional Te atoms form regular *2c-2e* bonds of 2.71 Å to 2.76 Å.

Two interpenetrating Te_3^{4-} units forming an almost square planar Te_5^{6-} unit with a central four-bonded Te atom are found in K_2SnTe_5 with distances of 3.02 Å and 3.06 Å [56]. These units can polymerize [57], the products of which will be discussed later in this manuscript. Adding two more Te atoms via single bonds, for example, results in bicyclic Te_7^{2-} [58].

2.2. Infinite motifs in polyselenides and polytellurides

2.2.1. One-dimensional motifs: chains

The above-mentioned fragments Q_n^{2-} and Q_n^{4-} can form higher dimensional arrays such as infinite chains, ribbons or layers. At least two bonds are required per *Q* atom in infinite chains, but the *Q* atoms may only participate in two *2c-2e* bonds, when their oxidation state is 0. Such neutral chains exist in the elements selenium and tellurium. On the other hand, Te is especially well known for its ability to form electron deficient multicenter bonds, thereby producing linear $^1_\infty[Te^-]$ chains. These chains occur in CuTe [59], UTe_2 [60] and $Ca_{0.66}K_4Te_3$ [61] with typical intrachain distances between

3.0 Å and 3.1 Å. These interactions are delocalized *2c-1e* ("half") bonds, wherein one *p* orbital is half-filled, indicating a one-dimensional metal.

Figure 4. Infinite Te^{1-} chains in $Ca_{0.5}K_4Te_3$ (left) and K_5Te_3 (right).

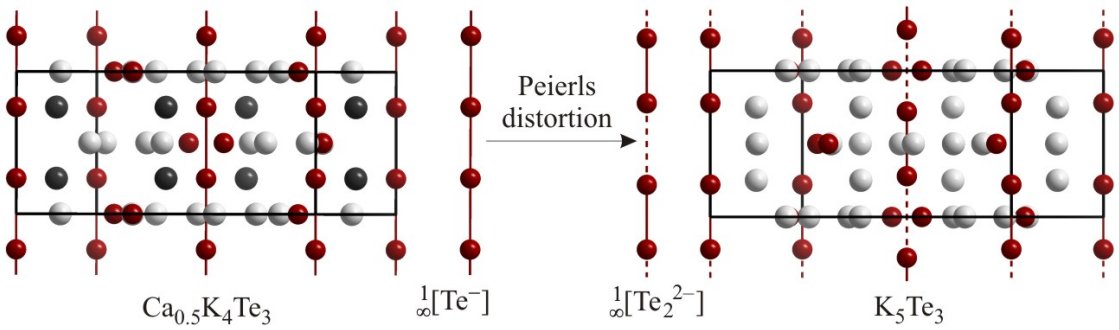

Such linear equidistant chains may undergo a Peierls distortion, i.e. exhibit alternating short and long distances, occurring with a metal-insulator transition (Figure 5) [62]. There are also examples of distorted linear chains of Te atoms with a formal charge of –1 such as in Cs_5Te_3 [63] or K_5Te_3 [64]. In these compounds, the Te atom chain features two different Te–Te distances, one of around 2.8 Å and the other larger than 3.5 Å. Thus, a description as $^1_\infty[Te_2^{2-}]$ is more appropriate for these compounds, wherein van der Waals forces connect the pairs to linear chains.

Figure 5. Peierls distortion of a linear $^1_\infty[Te^-]$ chain.

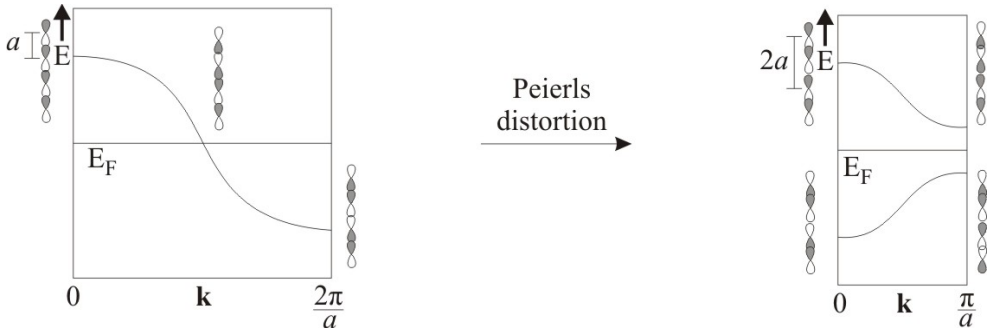

The dimorph TlTe is a nice example of a material exhibiting different Te atom chains [65]. The room temperature (RT) modification of TlTe represents an equidistant $^1_\infty[Te^-]$ chain with Te–Te distances of 3.08 Å. A parallel running, second linear equidistant Te atom chain within the same structure is more complex, as two additional Te atoms are connected to each chain atom via hypervalent bonds of 3.01 Å, yielding a $^1_\infty[Te_3^{3-}]$ chain (Figure 6). Thus, the RT modification may be written as $(Tl^+)_4Te_3^{3-}Te^-$. In the low temperature (LT, 172 K) modification, both chains are distorted. Every second $^1_\infty[Te_3^{3-}]$ chain is not equidistant with alternation distances of 2.86 Å and 3.30 Å, while the other $^1_\infty[Te_3^{3-}]$ remain undistorted. Moreover, the linear equidistant $^1_\infty[Te^-]$ chain of the RT form is slightly bent in the LT form. Overall, the LT phase may be viewed as $(Tl^+)_{16}Te_6^{6-}(Te_3^{3-})_2(Te^-)_4$.

Figure 6. Various Te atom chains of TlTe.

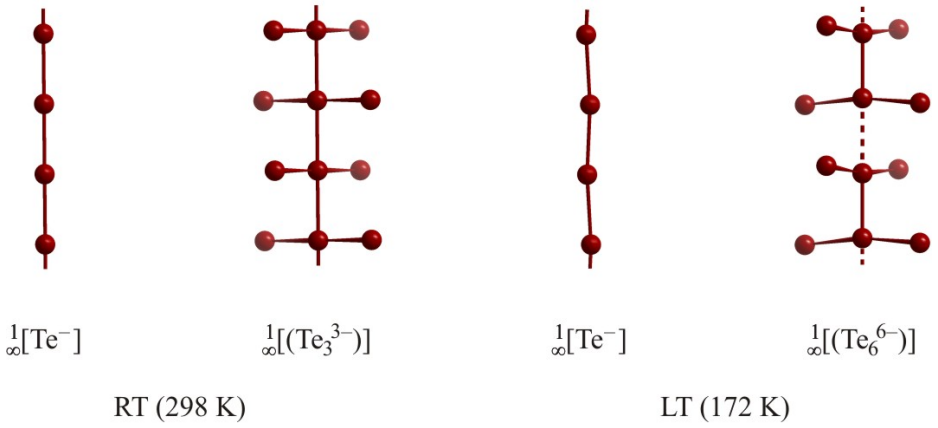

By reducing the number of valence electrons from 7 per atom in such a one-dimensional unit, the conditions become more and more complicated. The Te atoms in Tl_2Te_3, for example, have a valence electron concentration (VEC(Te)) of 6⅔, forming an infinite Te chain that can be described as polymerized linear Te_3^{4-} fragments (Figure 7). The bonds between the Te_3^{4-} units decrease the negative charges, leading to the description $^1_\infty[Te_3^{2-}]$ [66]. Two different distances were found in this chain due to different bonding situations. The short distance of 2.83 Å, a typical length for a *2c-2e* Te–Te bond, is found between the Te atoms of charge –½, the second distance (3.02 Å) occurs between Te^{1-} and $Te^{½-}$, indicative of a *3c-4e* bond.

Figure 7. Infinite Te atom chains with different VEC(Te) in Tl_2Te_3 (left), $LiTe_3$ (center) and Te (right).

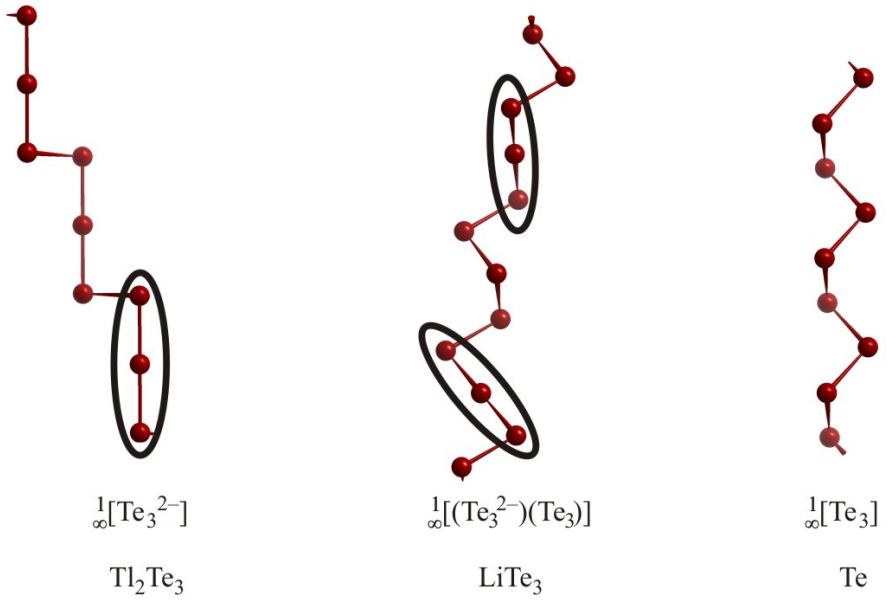

In $LiTe_3$ [67], the VEC(Te) within the chain is lowered to 6⅓. Consequently, this chain exhibits parts known from the Te atom chains in Tl_2Te_3 as well as from elemental Te [68], and can therefore be viewed as $^1_\infty[(Te_3)(Te_3^{2-})]$. The distances within this chain are 2.85 Å for the *2c-2e* bonds in the neutral

Te_3 part of the chain, 3.02 Å for the *3c-4e* bond in the Te_3^{2-} unit and 2.91 Å for the bond connecting these fragments.

2.2.2. One-dimensional motifs: Ribbons

Only very few polychalcogenides exist that contain one-dimensionally extended *Q* atom substructures with more than two *Q*–*Q* bonds per *Q* atom. The dialkali pentatellurides show two different forms of intercondensation of above-mentioned Te_5^{6-} squares to yield $^1_\infty[Te_5^{2-}]$ ribbons with VEC(Te) = 6.4, namely the *cis* conformation in Cs_2Te_5 [69] and the *trans* conformation in Rb_2Te_5 [70] (Figure 8).

Figure 8. Infinite Te ribbons with different modifications in Cs_2Te_5 (top left), Rb_2Te_5 (top right) and In_2Te_5 (bottom center).

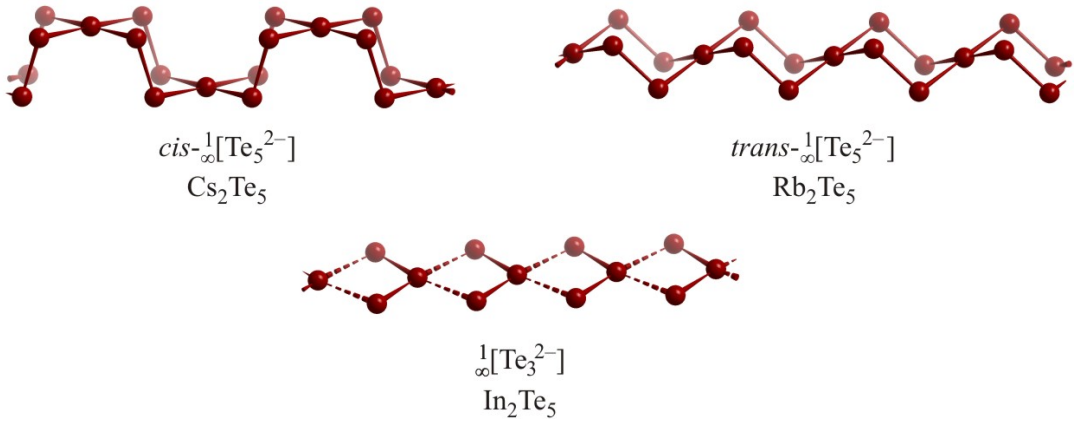

The distances in these ribbons range from 2.78 Å in Rb_2Te_5 and 2.77 Å in Cs_2Te_5 for the *2c-2e* bond between the Te_5 units to 3.04 Å in Rb_2Te_5 and 3.05 Å in Cs_2Te_5 for the *3c-4e* bond within the Te_5 units. In_2Te_5 [71] possesses a similar unit with a higher VEC(Te) of 6⅔, which causes a distortion, namely an alternation of short and long Te–Te distances of 2.83 Å (solid lines) and 3.36 Å (dashed lines). Therefore it is best described as a one-dimensional arrangement of Te_3^{2-} fragments.

2.2.3. Two-dimensional motifs: Layers

Compounds with hypervalently bonded Te atoms that are arranged in planar or puckered layers are often dominated by T-shaped fragments. These building blocks are then either directly connected to each other or bridged via other Te atoms. An overview of (schematic) T nets was published in the year 2004 [72]. One of the simplest examples of a T network containing Te atoms can be found in the planar layers of $NbTe_4$ [73]. Each Te atom in this layer is surrounded by three other Te atoms in form of a heavily distorted T. Four-membered rings, exhibiting Te–Te distances of 3.30 Å, are connected to surrounding four-membered rings via shorter bonds of 2.88 Å (Figure 9). This hole-style arrangement in $NbTe_4$ is subject to a distortion, driven by a charge density wave along the Nb atom chains perpendicular to the layer of interest. Considering the large difference of 0.4 Å between these distances, one could view this layer as loosely connected Te_2^{2-} units. This is in contrast to the Sb atom

layer of Hf_5Sb_9 [74], wherein all bonds are between 2.99 Å and 3.03 Å, i.e. all bonds of that T net are electron deficient multicenter bonds [75].

Figure 9. Different T nets in $NbTe_4$ (top left), $CsTe_4$ (top right) and Cs_3Te_{22} (bottom center).

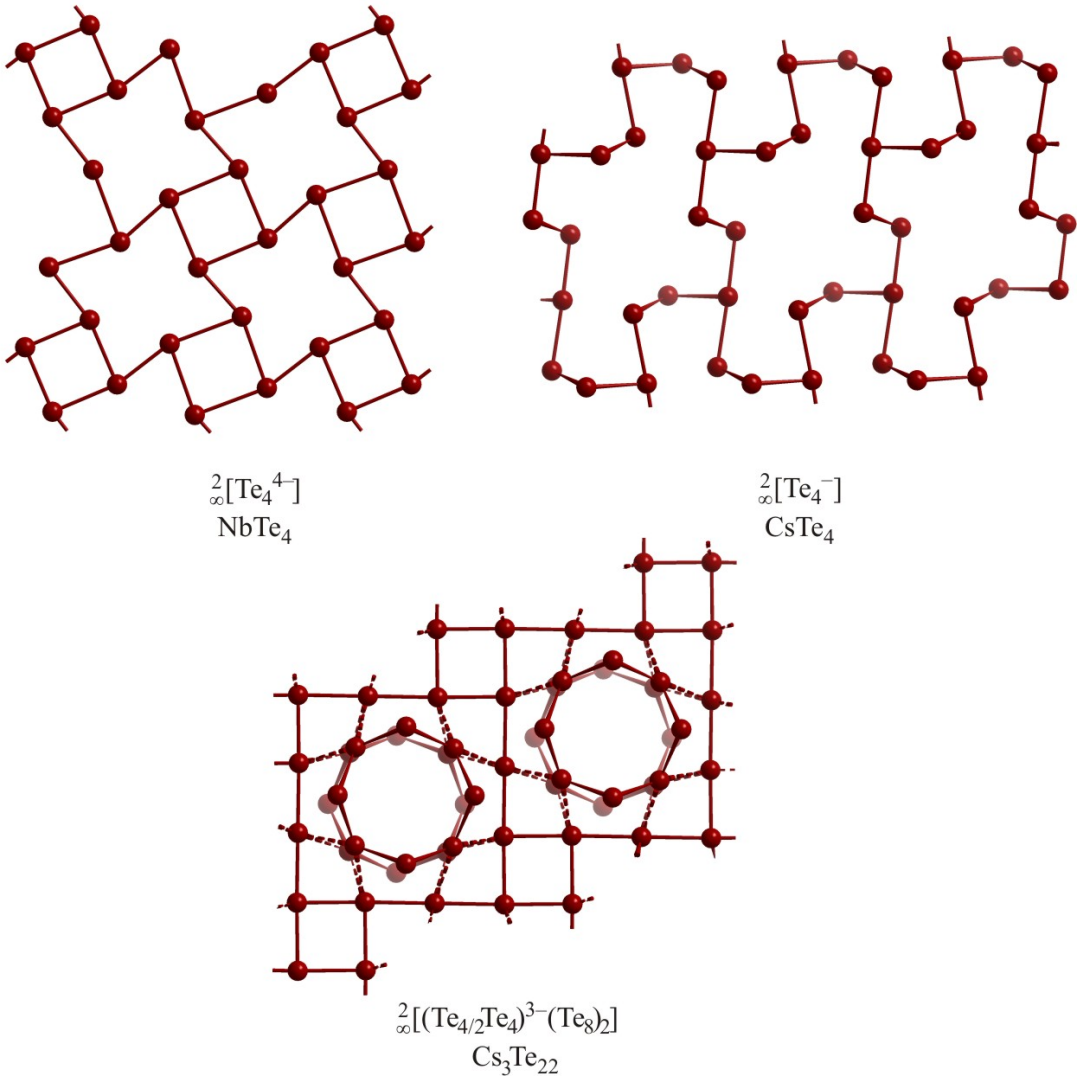

$CsTe_4$ [76] also features T-shaped Te atom units forming a layer, which is comprised of a polymerized Te_4^{4-} anion. This anion loses, due to this polymerization, three charges and builds a puckered layer that could be described as $^2_\infty[Te_4^{-}]$. The distances in the original T-shaped fragment in this layer are 2.92 Å and 3.14 Å for the collinear bonds, and 2.84 Å for the perpendicular bond. The connection between two (similar or different) fragments is slightly shorter (2.76 Å). The majority of the Te atoms are twofold coordinated and provide bonding angles between 96° and 103°. Therefore, the bonds within the Te_4^{4-} fragments could be considered as asymmetric *3c-4e* bonds and the remaining bonds as *2c-2e* bonds.

Cs_3Te_{22} provides an example of an electron-poor layer of Te atoms [77]. Cs_3Te_{22} contains also neutral eight-membered Te rings, and can be described as $(Cs^+)_3(Te_8)_2(Te_4Te_{4/2})^{3-}$. Its planar $^2_\infty[Te_4Te_{4/2}^{3-}]$ layer consists of two- and threefold connected Te atoms, with the former being linearly

coordinated and the latter T-shaped. The linearly bonded atoms interconnect the Te_4 squares comprising the T connected Te atoms. All Te–Te distances are between 3.00 Å and 3.07 Å. Band structure calculations indicate that this layer would be semiconducting with a charge of –4, but its actual charge of –3 renders it metallic [78].

2.2.4. Two-dimensional motifs: Chains connected to layers

The previously discussed lower dimensional fragments can be connected to two-dimensional layers in several ways. The binary chalcogenides UTe_2 [79], U_2Te_5 [80], α-UTe_3 [81] and ZrQ_3 [82,83] all contain linear chains aligned to form planar layers (Figure 10).

Figure 10. Planar layers of linear chains in U_2Te_5 (left), $ZrTe_3$ (center) and $ZrSe_3$ (right).

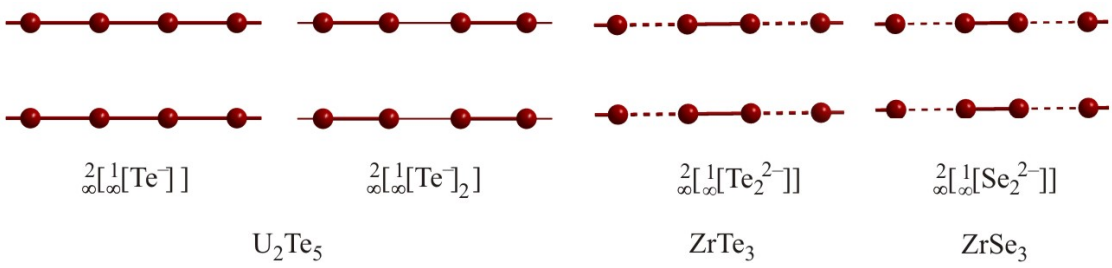

The structure of U_2Te_5 contains two different kinds of planar Te atom layers, i.e. $^2_\infty[^1_\infty[Te^-]]$ and $^2_\infty[^1_\infty[(Te^-)_2]]$. The $^2_\infty[^1_\infty[Te^-]]$ layer is sandwiched between two puckered [UTe] double layers, while two $^2_\infty[^1_\infty[(Te^-)_2]]$ layers are separated by a van der Waals gap and sandwiched between puckered double slabs. Both layers are comprised of linear chains with interchain distances of 4.18 Å. Within the $^2_\infty[^1_\infty[Te^-]]$ layer, almost equidistant intrachain bond lengths of 3.03 Å and 3.05 Å occur, while the $^2_\infty[^1_\infty[(Te^-)_2]]$ layer exhibits Te_2^{2-} pairs (2.90 Å) interconnected by longer interactions of 3.18 Å to a linear chain.

A very similar almost equidistant chain is found in UTe_2 as well (3.05 Å and 3.08 Å), while the distortion in α-UTe_3 is more severe with alternating distances of 2.75 Å and 3.35 Å. Similarly, the isostructural $ZrTe_3$ contains Te chains with alternating intrachain distances of 2.79 Å and 3.11 Å and interchain distances of 3.93 Å. The most severe distortion is present in the analogous $ZrSe_3$ with intrachain distances of 2.34 Å and 3.06 Å and an interchain distance of 3.77 Å.

Furthermore, many more complex variants, mostly tellurides, are known in this class, including UTe_5 [84], incommensurately modulated ALn_3Te_8 (*A* = K, Rb, Cs; *Ln* = La - Nd) [85], and $LnSeTe_2$ (*Ln* = La - Nd, Sm) [86], which exhibit corrugated chains interconnected to planar or slightly puckered layers. A detailed discussion of all these materials would go beyond the scope of this review; square nets and their distortions were featured in a review published in 2002 [21].

2.2.5. Two-dimensional motifs: oligomeric units connected to layers

An enormous variety of compounds contain fragments arranged to form layers, e.g. the Q_2^{2-} and Q_2^{3-} units. The structure of Cs_2Te_2 [87] features Te_2^{2-} dumbbells with a Te–Te distance of 2.78 Å, arranged in a herringbone-like pattern (Figure 11), and stacked between layers of cesium atoms. The distances between these dumbbells of 4.71 Å and 5.01 Å are too long for bonding interactions.

Another planar layer formation only consisting of Te_2^{2-} dumbbells (d_{Te-Te} = 2.78 Å) occurs in the crystal structure of *ALn*Te_4 [88,89] with an interpair distance of 3.50 Å, which is shorter than a van der Waals contact.

Figure 11. Layers of oligomeric Te atom fragments in Cs_2Te_2 (top left), *ALn*Te_4 (top right), $RbTe_6$ (bottom left), and $CrTe_3$ (bottom right).

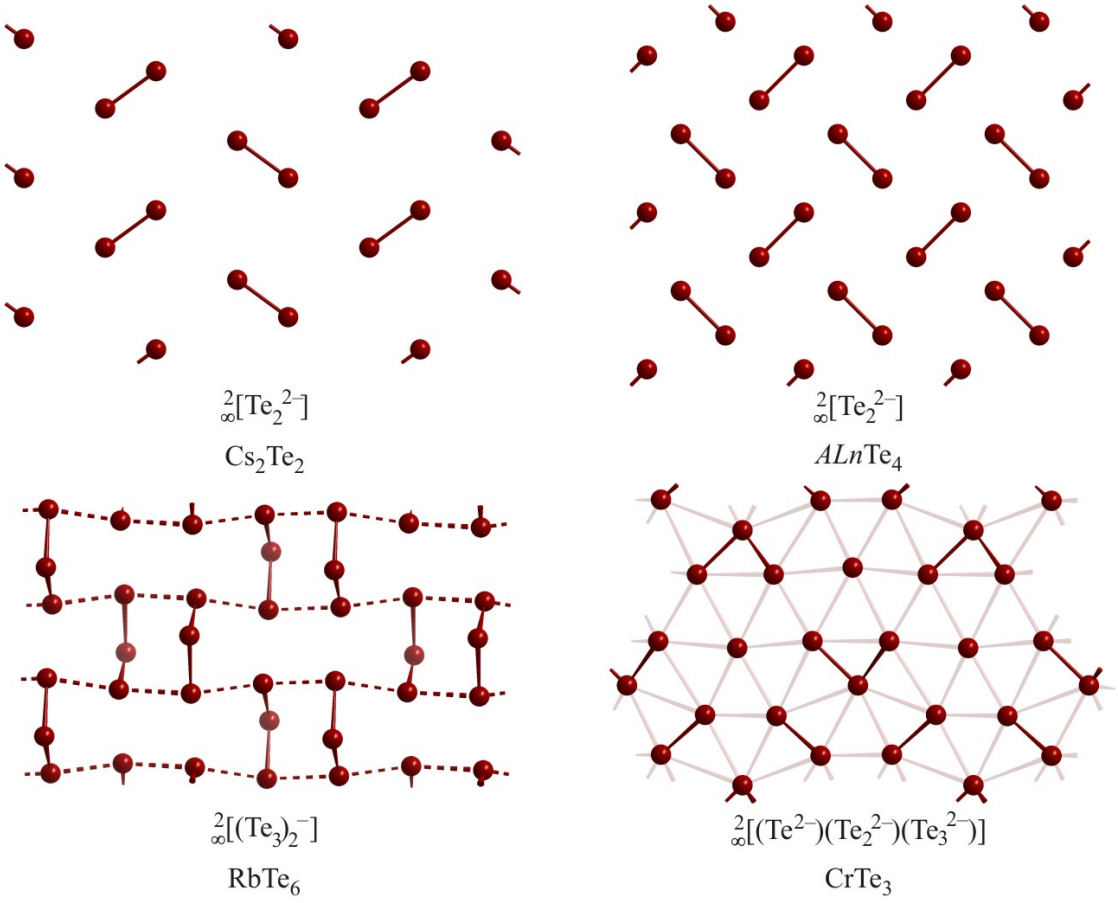

The structure of $RbTe_6$ [90] features a $^2_\infty[Te_6^{-}]$ layer that is puckered because of its bent Te_3 units, where the central Te atom takes a position either beneath or above the layer plane. Within these bent Te_3 units, the Te–Te distances are 2.78 Å and 2.79 Å, respectively, with a bond angle of 102°, while the distances between these units are 3.20 Å and 3.21 Å. The charge of the $^2_\infty[Te_6^{-}]$ layer cannot be readily understood; ignoring the 3.2 Å distances would indicate a charge of –2 for each Te_3 unit, while treating them as hypervalent half bonds would ideally result in neutral Te_3 units.

The structure of $CrTe_3$ contains Te atoms in three different oxidation states in a nearly planar layer [91]. The $^2_\infty[Te_3^{3-}]$ layer of this compound contains Te^{2-} ions and Te_2^{2-} and Te_3^{2-} units, with typical Te–Te distances of 2.82 Å. The assignment of charges is straightforward and yields a balanced formula for Cr in its +3 state: $(Cr^{3+})_2Te_3^{2-}Te_2^{2-}Te^{2-}$.

2.2.6. Three-dimensional motifs

The only known compound that is comprised of a three-dimensional, covalently bonded network of Te atoms is Cs_4Te_{28} [40]. The Te atom network is similar to the one in Cs_3Te_{22}, but in this case, half of the Te_8 rings are broken into Te_4 units that connect to one of the former linearly bonded atoms (Figure 12), which then assumes an oxidation state of zero.

Figure 12. Three-dimensional network of Te atoms in Cs_4Te_{28}.

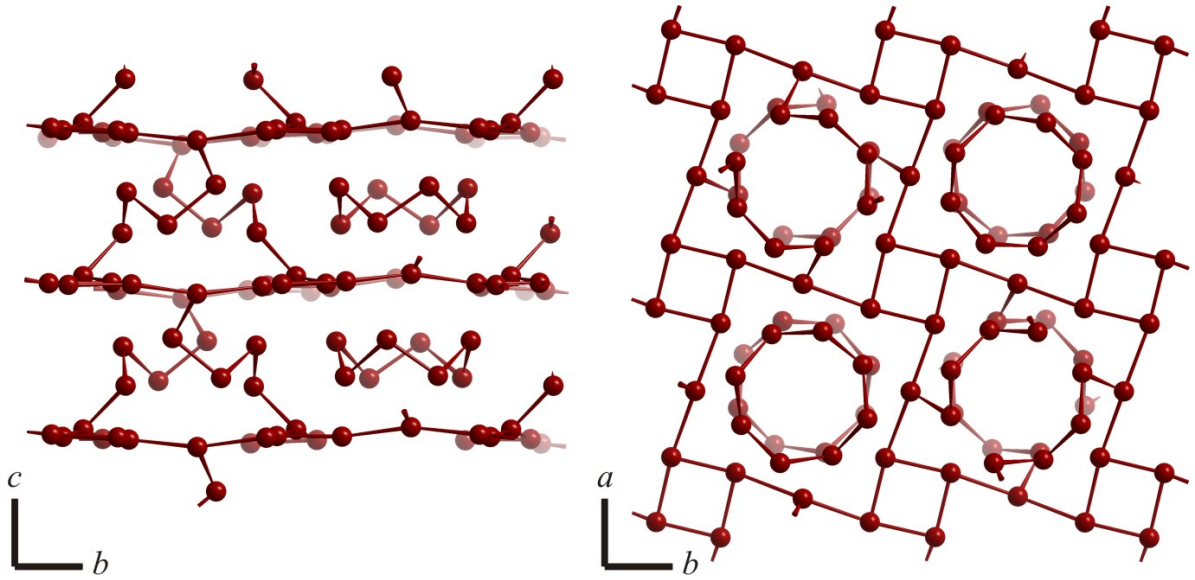

This covalently bonded three-dimensional network could be considered as $(Cs^+)_4Te_8[(Te_4)_{4/2}(Te_4Te_{4/2})_2^{4-}]$, wherein the neutral Te_8 ring is comprised of typical *2c-2e* bonds (2.79 Å - 2.83 Å) like elemental sulfur. The Te–Te bonds of the connecting (also neutral) Te_4 fragments are comparable (2.77 Å and 2.79 Å), as are the connections of these Te_4 units of 2.80 Å with the layer of Te atoms. As a result of the connection with the Te_4 units, all Te atoms of the layer are connected in a T-like shape exhibiting hypervalent bonds >2.9 Å, in contrast to the twofold linearly connected Te atoms in the structure Cs_3Te_{22}.

3. Conclusions

An overview of the variety of Se–Se and Te–Te interactions occurring in the solid state of both inorganic and organic polychalcogenides was presented. In contrast to polysulfides, the Se and Te atoms are capable of forming electron deficient multicenter (hypervalent) bonds. This adds significantly to the connectivity possibilities, e.g. the formation of T-shaped Te motifs or linear Se/Te fragments, which in turn increases the complexity of these polychalcogenides, a desired feature for, e.g., thermoelectric materials.

The tendency of Te towards higher coordination numbers is reflected in the higher abundance of complex Te atom layers, compared to Se. However, within the oligomeric units, the selenides and tellurides are quite comparable, so that more polyselenides with related two-dimensional motifs are likely to be uncovered in the near future as well.

Acknowledgements

Financial support from NSERC, CFI, OIT (Ontario Distinguished Researcher Award for H.K.), and the Canada Research Chair program (CRC for H.K.) is appreciated. Acknowledgment is made to the Donors of the American Chemical Society Petroleum Research Fund for partial support of this research.

References and Notes

1. Kosbar, L.L.; Murray, C.E.; Copel, M.; Afzali, A.; Mitzi, D.B. High-mobility ultrathin semiconducting films prepared by spin coating. *Nature* **2004**, *428*, 299-303.
2. Lange, S.; Nilges, T. $Ag_{10}Te_4Br_3$: A new silver(I) (poly)chalcogenide halide solid electrolyte. *Chem. Mater.* **2006**, *18*, 2538-2544.
3. Zheng, N.; Bu, X.; Feng, P. Synthetic design of crystalline inorganic chalcogenides exhibiting fast-ion conductivity. *Nature* **2003**, *426*, 428-432.
4. Tarascon, J.-M.; Armand, M. Issues and challenges facing rechargeable lithium batteries. *Nature* **2001**, *414*, 359-367.
5. Atwood, G. Phase-change materials for electronic memories. *Science* **2008**, *321*, 210-211.
6. Lencer, D.; Salinga, M.; Grabowski, B.; Hickel, T.; Neugebauer, J.; Wuttig, M. A map for phase-change materials. *Nat. Mater.* **2008**, *7*, 972-977.
7. Yamada, N.; Wuttig, M. Phase-change materials for rewriteable data storage. *Nat. Mater.* **2007**, *6*, 824-832.
8. Zakery, A.; Elliott, S.R. Optical properties and applications of chalcogenide glasses: A review. *J. Non-Cryst. Sol.* **2003**, *330*, 1-12.
9. Lowhorn, N.D.; Tritt, T.M.; Abbott, E.E.; Kolis, J.W. Enhancement of the power factor of the transition metal pentatelluride $HfTe_5$ by rare-earth doping. *Appl. Phys. Lett.* **2006**, *88*, 022101:1-022101:3.
10. Rowe, D.M. *Thermoelectrics Handbook: Macro to Nano*; CRC Press, Taylor & Francis Group: Boca Raton, FL, USA, 2006.
11. Sootsman, J.R.; Kong, H.; Uher, C.; D'Angelo, J.J.; Wu, C.-I.; Hogan, T.P.; Caillat, T.; Kanatzidis, M.G. Large enhancements in the thermoelectric power factor of bulk PbTe at high temperature by synergistic nanostructuring. *Angew. Chem. Int. Ed.* **2008**, *47*, 8618-8622.
12. Xu, H.; Kleinke, K.M.; Holgate, T.; Zhang, H.; Su, Z.; Tritt, T.M.; Kleinke, H. Thermoelectric performance of $Ni_yMo_3Sb_{7-x}Te_x$ ($y \leq 0.1$, $1.5 \leq x \leq 1.7$). *J. Appl. Phys.* **2009**, *105*, 053703:1-053703:5.
13. Böttcher, P.; Getzschmann, J.; Keller, R. Zur Kenntnis der Dialkalimetalldichalkogenide β-Na_2S_2, K_2S_2, α-Rb_2S_2, β-Rb_2S_2, K_2Se_2, Rb_2Se_2, α-K_2Te_2, β-K_2Te_2 und Rb_2Te_2. *Z. Anorg. Allg. Chem.* **1993**, *619*, 476-478.
14. Schäfer, H.; Eisenmann, B.; Müller, W. Zintl Phases: Transitions between metallic and ionic bonding. *Angew. Chem. Int. Ed. Engl.* **1973**, *12*, 694-712.
15. Nesper, R. Zintl-phases containing Li. *Prog. Solid State Chem.* **1990**, *20*, 1-45.
16. Kauzlarich, S.M. *Chemistry, Structure, and Bonding of Zintl Phases and Ions*; VCH: New York, NY, USA, 1996.
17. Siegel, S.G. Crystallographic studies of XeF_2 and XeF_4. *J. Am. Chem. Soc.* **1963**, *85*, 240-240.

18. Curnow, O.J. A Simple qualitative molecular-orbital/valence-bond description for the bonding in main group "hypervalent" molecules. *J. Chem. Educ.* **1998**, *75*, 910-915.
19. Papoian, G. A.; Hoffmann, R. Hypervalent bonding in one, two, and three dimensions: Extending the Zintl-Klemm concept to nonclassical electron-rich networks. *Angew. Chem. Int. Ed.* **2000**, *39*, 2408-2448.
20. Böttcher, P. Tellurium-Rich Tellurides. *Angew. Chem. Int. Ed. Engl.* **1988**, *27*, 759-772.
21. Patschke, R.; Kanatzidis, M.G. Polytelluride compounds containing distorted nets of tellurium. *Phys. Chem. Chem. Phys.* **2002**, *4*, 3266-3281.
22. Xu, J.; Kleinke, H. Unusual Sb–Sb bonding in high temperature thermoelectric materials. *J. Comput. Chem.* **2008**, *29*, 2134-2143.
23. Kanatzidis, M.G. From cyclo-Te_8 to Te_x^{n-} Sheets: Are Nonclassical Polytellurides More Classical than We Thought? *Angew. Chem. Int. Ed. Engl.* **1995**, *34*, 2109-2111.
24. Böttcher, P.; Doert, T. Chalcogen-rich chalcogenides: from the first ideas to a still growing field of research. *Phosphorus, Sulfur, Silicon* **1998**, *136-138*, 255-282.
25. Smith, D.M.; Ibers, J.A. Syntheses and solid-state structural chemistry of polytelluride anions. *Coord. Chem. Rev.* **2000**, *200-202*, 187-205.
26. Föppl, H.; Busmann, E.; Frorath, F.K. Die Kristallstrukturen von α-Na_2S_2 und K_2S_2, β-Na_2S_2 und Na_2Se_2. *Z. Anorg. Allg. Chem.* **1962**, *314*, 12-29.
27. Batchelor, R.J.; Einstein, F.W.B.; Gay, I.D.; Jones, C.H.W.; Sharma, R.D. Syntheses and solid-state NMR of tetrabutylammonium hydrogen telluride, tetramethylammonium hydrogen selenide and bis(tetramethylammonium) ditelluride and x-ray crystal structures of Me_4NSeH and $(Me_4N)_2Te_2$. *Inorg. Chem.* **1993**, *32*, 4378-4383.
28. Thiele, K.-H.; Steinicke, A.; Dümichen, U.; Neumüller, B. Darstellung und Reaktionen von Natriumtellurid, Na_2Te - Kristallstruktur von $[Na(CH_3OH)_3]_2Te_2$. *Z. Anorg. Allg. Chem.* **1996**, *622*, 231-234.
29. Pauling, L. *The Nature of the Chemical Bond*, 3rd ed.; Cornell University Press: Ithaca, NY, USA, 1948.
30. Böttcher, P. Die Kristallstruktur von K_2S_3 und K_2Se_3. *Z. Anorg. Allg. Chem.* **1977**, *432*, 167-172.
31. Assoud, A.; Soheilnia, N.; Kleinke, H. Band gap tuning in new strontium seleno-stannates. *Chem. Mater.* **2004**, *16*, 2215-2221.
32. Assoud, A.; Soheilnia, N.; Kleinke, H. The new semiconducting polychalcogenide Ba_2SnSe_5 exhibiting Se_3^{2-} units and distorted $SnSe_6$ octahedra. *J. Solid State Chem.* **2005**, *178*, 1087-1093.
33. Eisenmann, B.; Schäfer, H. K_2Te_3: The first binary alkali-metal polytelluride with Te_3^{2-} ions. *Angew. Chem. Int. Ed. Engl.* **1978**, *17*, 684.
34. Cui, Y.; Assoud, A.; Xu, J.; Kleinke, H. Structures and Physical Properties of new Semiconducting gold and copper polytellurides: $Ba_7Au_2Te_{14}$ and $Ba_{6.76}Cu_{2.42}Te_{14}$. *Inorg. Chem.* **2007**, *46*, 1215-1221.
35. Getzschmann, J.R.; Rönsch, E.; Böttcher, P. Crystal structure of dinatriumtetraselenide, Na_2Se_4. *Z. Kristallogr. -NCS* **1997**, *212*, 87.
36. Huffman, J.C.; Haushalter, R.C. Preparation and crystal structure of $(Ph_4P)_2Te_4 \cdot 2CH_3OH$. *Z. Anorg. Allg. Chem.* **1984**, *518*, 203-209.
37. Müller, V.; Frenzen, G.; Dehnicke, K.; Fenske, D. Synthese, FIR-Spektren und Kristallstrukturen der Pentaselenide K_2Se_5 und $(Na(15\text{-Krone-}5))_2Se_5$. *Z. Naturforsch. B* **1992**, *47*, 205-210.

38. Weller, F.; Adel, J.; Dehnicke, K. Polyselenide mit langkettigen Tetraalkylammoniumionen. Die Kristallstruktur von Trimethyl-tetradecyl-ammonium-hexaselenid. *Z. Anorg. Allg. Chem.* **1987**, *548*, 125-132.
39. Warren, C.J.; Haushalter, R.C.; Bocarsly, A.B. Electrochemical synthesis of a pseudo-two-dimensional polytelluride containing Te_{12}^{2-} anions: Structure of $[(C_2H_5)_4N]_2Te_{12}$. *J. Alloys Compd.* **1996**, *233*, 23-29.
40. Sheldrick, W.S.; Wachhold, M. Synthesis and structure of Cs_2Te_{13} and Cs_4Te_{28}, tellurium-rich tellurides on the methanolothermal route to Cs_3Te_{22}. *Chem. Commun.* **1996**, 607-608.
41. Assoud, A.; Xu, J.; Kleinke, H. Structures and physical properties of new semiconducting polyselenides $Ba_2Cu_\delta Ag_{4-\delta}Se_5$ with unprecedented linear Se_3^{4-} units. *Inorg. Chem.* **2007**, *46*, 9906-9911.
42. Dürichen, P.; Bolte, M.; Bensch, W. Synthesis, crystal structure, and properties of polymeric $Rb_{12}Nb_6Se_{35}$, a novel ternary niobium selenide consisting of infinite anionic chains built up by Nb_2Se_{11} units containing an uncommon Se_3^{4-}-fragment. *J. Solid State Chem.* **1998**, *140*, 97-102.
43. Tasman, H.A.; Boswijk, K.H. Reinvestigation of the crystal structure of CsI_3. *Acta Crystallogr.* **1955**, *8*, 59-60.
44. Mooney-Slater, R.C.L. The triiodide ion in tetraphenylarsonium triiodide. *Acta Crystallogr.* **1959**, *12*, 187-196.
45. Rundle, R.E. On the Problem Structure of XeF_4 and XeF_2. *J. Am. Chem. Soc.* **1963**, *85*, 112-113.
46. Cordier, G.; Schäfer, H.; Stelter, M. Darstellung und Struktur der Verbindung $Ca_{14}AlSb_{11}$. *Z. Anorg. Allg. Chem.* **1984**, *519*, 183-188.
47. Kim, H.; Olmstead, M.M.; Klavins, P.; Webb, D.J.; Kauzlarich, S.M. Structure, magnetism, and colossal magnetoresistance (CMR) of the ternary transition metal solid solution $Ca_{14-x}Eu_xMnSb_{11}$ ($0 < x < 14$). *Chem. Mater.* **2002**, *14*, 3382-3390.
48. Brown, S.R.; Kauzlarich, S.M.; Gascoin, F.; Snyder, G.J. $Yb_{14}MnSb_{11}$: New high efficiency thermoelectric material for power generation. *Chem. Mater.* **2006**, *18*, 1873-1877.
49. Lu, Y.; Ibers, J.A. Synthesis and characterization of the new quaternary one-dimensional chain materials, potassium copper niobium selenides, $K_2CuNbSe_4$ and $K_3CuNb_2Se_{12}$. *Inorg. Chem.* **1991**, *30*, 3317-3320.
50. Sunshine, S.A.; Ibers, J.A. Redetermination of the structures of $CuTaS_3$ and Nb_2Se_9. *Acta Crystallogr. C* **1987**, *43*, 1019-1022.
51. Böttcher, P.; Keller, R. The crystal structure of NaTe and its relationship to tellurium-rich tellurides. *J. Less-Common Met.* **1985**, *109*, 311-321.
52. Assoud, A.; Derakhshan, S.; Soheilnia, N.; Kleinke, H. Electronic structure and physical properties of the semiconducting polytelluride Ba_2SnTe_5 with a unique Te_5^{4-} unit. *Chem. Mater.* **2004**, *16*, 4193-4198.
53. Apblett, A.; Grein, F.; Johnson, J.P.; Passmore, J.; White, P.S. Preparation and X-ray crystal structure of $[I_5^+][AsF_6^-]$, an electronic structure of the I_5^+ cation. *Inorg. Chem.* **1986**, *25*, 422-426.
54. McConnachie, J.M.; Ansari, M.A.; Bollinger, J.C.; Salm, R.J.; Ibers, J.A. Synthesis and structural characterization of the telluroargentate $[PPh_4]_2[NEt_4][AgTe_7]$ and telluromercurate $[PPh_4]_2[HgTe_7]$ compounds containing the unprecedented η_3-Te_7^{4-} polytelluride anion. *Inorg. Chem.* **1993**, *32*, 3201-3202.

55. Smith, D.M.; Roof, L.C.; Ansari, M.A.; McConnachie, J.M.; Bollinger, J.C.; Pell, M.A.; Salm, R.J.; Ibers, J.A. Synthesis, reactivity, and structural characterization of the nonclassical $[MTe_7]^{n-}$ Anions (M = Ag, Au, n = 3; M = Hg, n = 2). *Inorg. Chem.* **1996**, *35*, 4999-5006.
56. Eisenmann, B.; Schwerer, H.; Schäfer, H. Plane, zu Ketten verknüpfte Te_5^{6-}-Anionen im K_2SnTe_5. *Mat. Res. Bull.* **1983**, *18*, 383-387.
57. Bernstein, J.; Hoffmann, R. Hypervalent Tellurium in One-Dimensional Extended Structures Containing Te_5^{n-} Units. *Inorg. Chem.* **1985**, *24*, 4100-4108.
58. Harbrecht, B.; Selmer, A. Rhenium selenide tellurides $Re_2Se_xTe_{5-x}$: The structure of $Re_6Se_8Te_7$. *Z. Anorg. Allg. Chem.* **1994**, *620*, 1861-1866.
59. Anderko, K.; Schubert, K. Untersuchungen im System Kupfer-Tellur. *Z. Metallk.* **1954**, *45*, 371-378.
60. Klein-Haneveld, A.J.; Jellinek, F. The crystal structure of stoichiometric uranium ditelluride. *J. Less-Common Met.* **1970**, *21*, 45-49.
61. Schewe-Miller, I.; Böttcher, P. Ternäre Telluride mit W_5Si_3-Typ-Struktur: $M_xK_4Te_3$ (M=Ca, Sr). *J. Alloys Compd.* **1992**, *183*, 98-108.
62. Peierls, R.E. *Quantum Theory of Solids*; Clarendon Press: Oxford, UK, 1955.
63. Schewe-Miller, I.; Böttcher, P. Synthesis and crystal structures of K_5Se_3, Cs_5Te_3 and Cs_2Te. *Z. Kristallogr.* **1991**, *196*, 137-151.
64. Schewe-Miller, I.; Böttcher, P. Darstellung und Kristallstruktur des K_5Te_3. *Z. Naturforsch. B* **1990**, *45*, 417-422.
65. Stöwe, K. The Phase Transition of TlTe: Crystal Structure. *J. Solid State Chem.* **2000**, *149*, 123-132.
66. Doert, T.; Cardoso Gil, R.H.; Böttcher, P. The crystal structure of Tl_2Te_3 - a reinvestigation. *Z. Anorg. Allg. Chem.* **1999**, *625*, 2160-2163.
67. Valentine, D.Y.; Cavin, O.B.; Yakel, H.L., Jr. On the crystal structure of $LiTe_3$. *Acta Crystallogr. B* **1977**, *33*, 1389-1396.
68. Bradley, A.J. The crystal structure of Te. *Philos. Mag.* **1924**, *48*, 477-496.
69. Böttcher, P.; Kretschmann, U. Darstellung und Kristallstruktur von Dicaesiumpentatellurid Cs_2Te_5. *Z. Anorg. Allg. Chem.* **1982**, *491*, 39-46.
70. Böttcher, P.; Kretschmann, U. Darstellung und Kristallstruktur von Dirubidiumpentatellurid, Rb_2Te_5. *J. Less-Common Met.* **1983**, *95*, 81-91.
71. Sutherland, H.H.; Hogg, J.H.C.; Walton, P.D. Indium polytelluride In_2Te_5. *Acta Crystallogr. B* **1976**, *32*, 2539-2541.
72. Ienco, A.; Proserpio, D. M.; Hoffmann, R. Main group element nets to a T. *Inorg. Chem.* **2004**, *43*, 2526-2540.
73. Böhm, H.; von Schnering, H.G. The modulated structure of niobium tetratelluride $NbTe_4$. *Z. Kristallogr.* **1985**, *171*, 41-64.
74. Assoud, A.; Kleinke, K.M.; Soheilnia, N.; Kleinke, H. T-shaped nets of Sb atoms in the binary antimonide Hf_5Sb_9. *Angew. Chem. Int. Ed.* **2004**, *43*, 5260-5262.
75. Xu, J.; Kleinke, K.M.; Kleinke, H. electronic structure and physical properties of Hf_5Sb_9 containing a unique T net of Sb atoms. *Z. Anorg. Allg. Chem.* **2008**, *634*, 2367-2372.
76. Böttcher, P.; Kretschmann, U. Darstellung und Kristallstruktur von $CsTe_4$. *Z. Anorg. Allg. Chem.* **1985**, *523*, 145-152.

77. Sheldrick, W.S.; Wachhold, M. Discrete crown-shaped Te_8 rings in Cs_3Te_{22}. *Angew. Chem. Int. Ed. Engl.* **1995**, *34*, 450-451.
78. Liu, Q.; Goldberg, N.; Hoffmann, R. A 2,3-connected tellurium net and the Cs_3Te_{22} phase. *Chem. Eur. J.* **1996**, *2*, 390-7.
79. Stöwe, K. Contributions to the crystal chemistry of uranium tellurides. III. Temperature-dependent structural investigations on uranium ditelluride. *J. Solid State Chem.* **1996**, *127*, 202-210.
80. Stöwe, K. Beiträge zur Kristallchemie der Urantelluride. II. Die Kristallstruktur des Diuranpentatellurids U_2Te_5. *Z. Anorg. Allg. Chem.* **1996**, *622*, 1423-1427.
81. Stöwe, K. Beiträge zur Kristallchemie der Urantelluride. I. Die Kristallstruktur des α-Urantritellurids. *Z. Anorg. Allg. Chem.* **1996**, *622*, 1419-1422.
82. Krönert, W.; Plieth, K. Die Struktur des Zirkontriselenids $ZrSe_3$. *Z. Anorg. Allg. Chem.* **1965**, *336*, 207-218.
83. Felser, C.; Finckh, E.W.; Kleinke, H.; Rocker, F.; Tremel, W. Electronic properties of $ZrTe_3$. *J. Mater. Chem.* **1998**, *8*, 1787-1798.
84. Noel, H. Crystal structure of the low-dimensional uranium pentatulluride: UTe_5. *Inorg. Chim. Acta* **1985**, *109*, 205-207.
85. Patschke, R.; Heising, J.; Schindler, J. L.; Kannewurf, C. R.; Kanatzidis, M. Site occupancy wave and unprecedented infinite zigzag $(Te_2^{2-})_n$ chains in the flat Te nets of the new ternary rare earth telluride family. *J. Solid State Chem.* **1998**, *135*, 111-115.
86. Fokwa, B.P.T.; Doert, T. The ternary rare-earth polychalcogenides $LaSeTe_2$, $CeSeTe_2$, $PrSeTe_2$, $NdSeTe_2$, and $SmSeTe_2$: Syntheses, crystal structures, electronic properties, and charge-density-wave-transitions. *Solid State Sci.* **2005**, *7*, 573-587.
87. Getzschmann, J.; Böttcher, P.; Kaluza, W. Darstellung und Kristallstrukturen von β-Rb_2Te_2 und Cs_2Te_2 sowie die Verfeinerung der Strukturen von Ca_2P_2 und Sr_2As_2. *Z. Kristallogr.* **1996**, *211*, 90-95.
88. Dürichen, P.; Bensch, W. Cesium gadolinium tetratelluride. *Acta Crystallogr. C* **1997**, *53*, 267-269.
89. Stöwe, K. Syntheses and crystal structures of $KPrTe_4$, $KGdTe_4$ and $RbGdTe_4$. *Solid State Sci.* **2003**, *5*, 765-769.
90. Sheldrick, W.S.; Schaaf, B. $RbTe_6$, ein Polytellurid mit Schichtstruktur $[Te_6^-]$ *Z. Naturforsch. B* **1994**, *49*, 993-996.
91. Klepp, K.O.; Ipser, H. $CrTe_3$ - A novel transition-Metal polytelluride. *Angew. Chem. Int. Ed. Engl.* **1982**, *21*, 911-911.

Sample Availability: Not available.